J|A|C|S
ARTICLES
Published on Web 05/12/2007

Double-Lanthanide-Binding Tags: Design, Photophysical Properties, and NMR Applications

Langdon J. Martin,[†] Martin J. Hähnke,[‡] Mark Nitz,[†] Jens Wöhnert,[‡] Nicholas R. Silvaggi,[§] Karen N. Allen,[§] Harald Schwalbe,*[,‡] and Barbara Imperiali*[,†]

Contribution from the Departments of Chemistry and Biology, Massachusetts Institute of Technology, 77 Massachusetts Avenue, Cambridge, Massachusetts 02139, Institut für Organische Chemie und Chemische Biologie, Center for Biomolecular Magnetic Resonance, Johann Wolfgang Goethe-Universität Frankfurt, Max-von-Laue-Strasse 7, 60438 Frankfurt/M, Germany, and Department of Physiology and Biophysics, Boston University School of Medicine, 715 Albany Street, Boston, Massachusetts 02118

Received January 22, 2007; E-mail: imper@mit.edu; schwalbe@nmr.uni-frankfurt.de

Abstract: Lanthanide-binding tags (LBTs) are peptide sequences of up to 20 encoded amino acids that tightly and selectively complex lanthanide ions and can sensitize terbium (Tb^{3+}) luminescence. On the basis of these properties, it was predicted that increasing the number of bound lanthanides would improve the capabilities of these tags. Therefore, using a structurally well-characterized single-LBT sequence as a starting point, a "double-LBT" (dLBT), which concatenates two lanthanide-binding motifs, was designed. Herein we report the generation of dLBT peptides and luminescence and NMR studies on a dLBT-tagged ubiquitin fusion protein. These lanthanide-bound constructs are shown to be improved luminescent tags with avid lanthanide binding and up to 3-fold greater luminescence intensity. NMR experiments were conducted on the ubiquitin construct, wherein bound paramagnetic lanthanides were used as alignment-inducing agents to gain residual dipolar couplings, which are valuable restraints for macromolecular structure determination. Together, these results indicate that dLBTs will be valuable chemical tools for biophysical applications leading to new approaches for studying the structure, function, and dynamics of proteins.

Introduction

Tools for the study of protein structure, dynamics, and function are essential to all aspects of biology, biochemistry, and bioengineering. In this context, the diverse and versatile photophysical properties of trivalent lanthanide ions are gaining attention.[1−4] Many lanthanide ions exhibit luminescent properties with sharp, distinctive emission profiles, ranging from the visible region into the near-IR, and long luminescence lifetimes (microseconds to milliseconds). In these applications, the inherently low absorption of lanthanide ions, due to forbidden electron transitions, is readily overcome by an appropriately placed sensitizer-fluorophore.[5,6] Additionally, since most members of the series are paramagnetic (with the exception of La^{3+} and Lu^{3+}) and have an anisotropic susceptibility tensor, they can be used in NMR spectroscopy to partially orient proteins in the magnetic field.[7−9] This leads to magnetic dipolar interactions between adjacent spins that are otherwise averaged to zero in solution due to molecular tumbling. These residual dipolar couplings (RDCs) can be observed and have proven to yield useful long-range restraints for structure determination, since they depend on the orientation of the internuclear vector relative to the alignment frame induced by the bound lanthanide.[10,11] Finally, their strong anomalous scattering can be used to phase X-ray diffraction data.[12,13]

Various methods for the incorporation of lanthanide ions into biomolecules have been explored. In specialized applications, the similarity of trivalent lanthanides (Ln^{3+}) to divalent calcium (Ca^{2+}) in ionic radius and oxophilicity has enabled their direct incorporation into calcium-binding proteins.[8,12,14] The majority of proteins, however, lack native calcium-binding sites; therefore, one approach has been to incorporate lanthanide-chelating prosthetic groups as the side chain of non-natural amino acids[15] or via chemical modification of uniquely reactive amino acid

[†] Massachusetts Institute of Technology.
[‡] Johann Wolfgang Goethe-Universität Frankfurt.
[§] Boston University School of Medicine.

(1) Elbanowski, M.; Makowska, B. *J. Photochem. Photobiol. A* **1996**, *99*, 85−92.
(2) Handl, H. L.; Gillies, R. J. *Life Sci.* **2005**, *77*, 361−371.
(3) Hemmilae, I.; Laitala, V. *J. Fluoresc.* **2005**, *15*, 529−542.
(4) Bunzli, J.-C. G. *Acc. Chem. Res.* **2006**, *39*, 53−61.
(5) Gudgin Dickson, E. F.; Pollak, A.; Diamandis, E. P. *J. Photochem. Photobiol. B* **1995**, *27*, 3−19.
(6) Richardson, F. S. *Chem. Rev.* **1982**, *82*, 541−552.
(7) Veglia, G.; Opella, S. J. *J. Am. Chem. Soc.* **2000**, *122*, 11733−11734.
(8) Barbieri, R.; Bertini, I.; Cavallaro, G.; Lee, Y.-M.; Luchinat, C.; Rosato, A. *J. Am. Chem. Soc.* **2002**, *124*, 5581−5587.
(9) Pintacuda, G.; John, M.; Su, X.-C.; Otting, G. *Acc. Chem. Res.* **2007**, *40*, 206−212.
(10) Bertini, I.; Janik, M. B. L.; Liu, G.; Luchinat, C.; Rosato, A. *J. Magn. Reson.* **2001**, *148*, 23−30.
(11) Bertini, I.; Luchinat, C.; Parigi, G. *Concepts Magn. Reson.* **2002**, *14*, 259−286.
(12) Pidcock, E.; Moore, G. R. *J. Biol. Inorg. Chem.* **2001**, *6*, 479−489.
(13) Purdy, M. D.; Ge, P.; Chen, J.; Selvin, P. R.; Wiener, M. C. *Acta Crystallogr. D* **2002**, *D58*, 1111−1117.
(14) Burroughs, S. E.; Horrocks, W. D., Jr.; Ren, H.; Klee, C. B. *Biochemistry* **1994**, *33*, 10428−10436.
(15) Becker, C. F. W.; Clayton, D.; Shapovalov, G.; Lester, H. A.; Kochendoerfer, G. G. *Bioconjugate Chem.* **2004**, *15*, 1118−1124.

10.1021/ja070480v CCC: $37.00

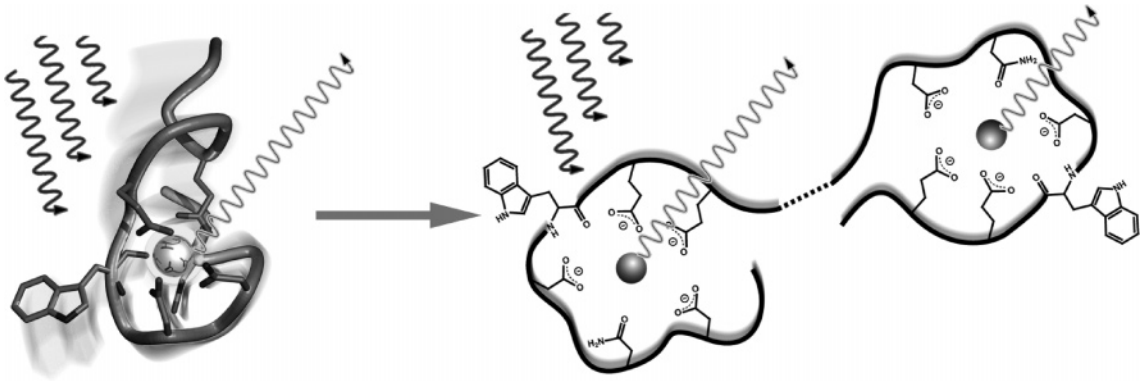

Figure 1. Representation of the design strategy for converting the single-LBT (sLBT) into the double-LBT (dLBT). The image depicts the peptide backbone based on the crystal structure of a single-LBT (**sLBT1**) previously determined.[23] The side chains that chelate Tb^{3+} are shown, along with the tryptophan-sensitizer with its Tb^{3+}-coordinating peptide-backbone carbonyl. The indole ring is excited at 280 nm, thereby sensitizing the Tb^{3+} which emits at 544 nm. The design goal for the dLBT is to incorporate two Tb^{3+}-binding sites within a contiguous sequence, potentially conferring advantages in luminescence output, X-ray scattering power, and anisotropic magnetic susceptibility, together with reduced mobility relative to the tagged protein due to the larger mass.

Table 1. Comparison of Tb^{3+}-Binding Affinity and Luminescence Intensity of Select Single-LBTs

single-LBT	position[a] –1	0	1	2	3	4	5	6	7	8	9	10	11	12	13	14	15	K_D (nM), Tb^{3+}	relative intensity[c]
sLBT1	Y	I	D	T	N	N	D	G	W	Y	E	G	D	E	L	L	A	57[b]	1.9
sLBT2	Y	I	D	T	N	N	D	G	W	I	E	G	D	E	L	L	A	38	1.0
sLBT3	F	I	D	T	N	N	D	G	W	I	E	G	D	E	L	L	A	18[b]	1.3

[a] The LBT residue-numbering system is based on the literature.[19,20] [b] These K_D values are taken from the published data.[22,24] [c] Luminescence comparison of equal concentrations of peptide saturated with Tb^{3+}.

residues such as cysteine.[13,16] While requiring considerable manipulation, these chelates can bind the lanthanide extremely tightly and may incorporate a sensitizer.

A straightforward and generalizable approach is to integrate a lanthanide-binding sequence as a protein co-expression tag via molecular biology strategies.[17,18] Utilizing information about calcium-binding loops,[19,20] recent design and engineering studies have resulted in the development of short polypeptides comprising 20 encoded amino acids or fewer that bind tightly and selectively to lanthanides.[21,22] These peptides, dubbed "lanthanide-binding tags" (LBTs, Figure 1), show low-nanomolar affinities and are selective for lanthanides over other common metal ions.[21−24] The protean nature of these tags as probes has been demonstrated by their use for luminescence-based visualization on gels,[21] as magnetic-field paramagnetic alignment agents in protein NMR experiments,[25,26] in fluorescence microscopy,[27] and as partners in luminescence resonance energy transfer (LRET) studies.[28]

While most applications of lanthanide ions in protein studies require only one metal ion per protein, a construct that selectively incorporates two ions could potentially confer advantages in luminescence output, X-ray scattering power, and anisotropic magnetic susceptibility. To this end, we have built upon our initial structure/function analyses with the single-LBT to design double-LBTs (dLBTs) that simultaneously bind and sensitize two lanthanide ions. Herein, we describe the generation and characterization of dLBT peptides, demonstrate their photophysical properties, and present their usage in NMR spectroscopy. In an accompanying paper, the crystallization and crystallographic analysis of a dLBT-containing protein is presented.[29] Through these studies, we shall highlight the superiority of the dLBT in these applications.

Results and Discussion

Design and Selection of the dLBT Sequence. The dLBT prototype was designed with the intent of balancing high terbium-ion affinity with strong luminescence. Figure 1 conceptualizes the dLBT design process. The crystal structure of a Tb^{3+}-bound single-LBT (**sLBT1**, Table 1) revealed that the side chains of residues at positions −1, 8, and 13 form a hydrophobic core.[23] A combinatorial library was therefore designed to optimize these residues.[24] Initial results yielded **sLBT2**, in which the tyrosine residue at position 8 was mutated to isoleucine (Table 1). Although the luminescence output of this LBT was reduced, the improved K_D prevailed in its selection as the

(16) Rodriguez-Castaneda, F.; Haberz, P.; Leonov, A.; Griesinger, C. *Magn. Reson. Chem.* **2006**, *44*, S10−S16 and references therein.
(17) MacKenzie, C. R.; Clark, I. D.; Evans, S. V.; Hill, I. E.; MacManus, J. P.; Dubuc, G.; Bundle, D. R.; Narang, S. A.; Young, N. M.; Szabo, A. G. *Immunotechnology* **1995**, *1*, 139−150.
(18) Vázquez-Ibar, J. L.; Weinglass, A. B.; Kaback, H. R. *Proc. Natl. Acad. Sci. U.S.A.* **2002**, *99*, 3487−3492.
(19) Marsden, B. J.; Hodges, R. S.; Sykes, B. D. *Biochemistry* **1988**, *27*, 4198−4206.
(20) MacManus, J. P.; Hogue, C. W.; Marsden, B. J.; Sikorska, M.; Szabo, A. G. *J. Biol. Chem.* **1990**, *265*, 10358−10366.
(21) Franz, K. J.; Nitz, M.; Imperiali, B. *ChemBioChem* **2003**, *4*, 265−271.
(22) Nitz, M.; Franz, K. J.; Maglathlin, R. L.; Imperiali, B. *ChemBioChem* **2003**, *4*, 272−276.
(23) Nitz, M.; Sherawat, M.; Franz, K. J.; Peisach, E.; Allen, K. N.; Imperiali, B. *Angew. Chem., Int. Ed.* **2004**, *43*, 3682−3685.
(24) Martin, L. J.; Sculimbrene, B. R.; Nitz, M.; Imperiali, B. *QSAR Comb. Sci.* **2005**, *24*, 1149−1157.
(25) Wöhnert, J.; Franz, K. J.; Nitz, M.; Imperiali, B.; Schwalbe, H. *J. Am. Chem. Soc.* **2003**, *125*, 13338−13339.
(26) Su, X.-C.; Huber, T.; Dixon, N. E.; Otting, G. *ChemBioChem* **2006**, *7*, 1599−1604.
(27) Goda, N.; Tenno, T.; Inomata, K.; Iwaya, N.; Sasaki, Y.; Shirakawa, M.; Hiroaki, H. *Biochim. Biophys. Acta* **2007**, *1773*, 141−146.
(28) Sculimbrene, B. R.; Imperiali, B. *J. Am. Chem. Soc.* **2006**, *128*, 7346−7352.
(29) Silvaggi, N. R.; Martin, L. J.; Schwalbe, H.; Imperiali, B.; Allen, K. N. *J. Am. Chem. Soc.* **2007**, *129*, 7114−7120.

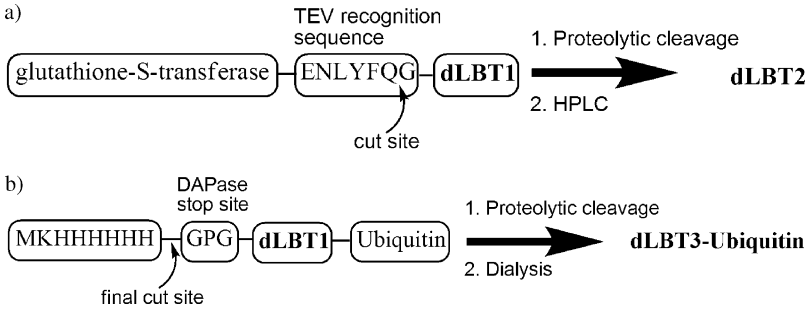

Figure 2. Generation of dLBTs. (a) Strategy for obtaining pure **dLBT2** peptide via GST fusion. (b) Strategy for generating the **dLBT3**-ubiquitin construct.

prototype for the first generation of dLBTs; the concatenation of two lanthanide-binding motifs was expected to compensate for the reduced luminescence. The link connecting the N- and C-terminal lanthanide-binding motifs was designed to preserve the interactions in the hydrophobic core. Position 13 of the N-terminal motif was set adjacent to position −1 of the C-terminal motif in order to promote intramolecular hydrophobic interactions, thereby creating the sequence for **dLBT1**: YIDTNNDGWIEGDELYIDTNNDGWIEGDELLA (Table 2).

Refinement of the lead from the combinatorial library, further optimizing the hydrophobic core, yielded **sLBT3** (Table 1), which included an additional mutation at position −1 (Tyr→Phe).[24] This sLBT showed improved terbium-binding affinity and luminescence; future studies on dLBTs may therefore take advantage of this mutation. It should be noted that not all applications of LBTs require a sensitizer (e.g., NMR and crystallography), and non-luminescent LBTs can be used successfully.[26] However, for maximum utility, it is advantageous to include a sensitizer for exploitation of the luminescence properties of the LBT.

Preparation of dLBT Peptides and a dLBT-Ubiquitin Construct. Initially, the prototype double-LBT (**dLBT1**, Table 2) was synthesized by solid-phase peptide synthesis. However, the efficiency of amino acid coupling became significantly reduced after the first 20 residues, leading to a number of truncation products that could not be separated from full-length **dLBT1**. Therefore, an alternate production strategy involving expression of the dLBT sequence as a fusion protein was pursued. Pure, full-length dLBT peptide was obtained via overexpression in *Escherichia coli* using a glutathione *S*-transferase (GST) fusion strategy. DNA encoding the dLBT was inserted into the pGEX-4T-2 plasmid (Amersham Biosciences) to generate the gene for a GST fusion protein with a C-terminal dLBT and an intervening mTEV protease recognition sequence. The fusion protein was overexpressed, purified, and cleaved with mTEV protease (Figure 2a). The protease cleavage site resulted in an additional N-terminal glycine residue, yielding **dLBT2** (Table 2), which was purified by HPLC (see Supporting Information).

The expression and purification of **dLBT3**-ubiquitin was carried out using standard molecular biology and protein chemistry methods (Figure 2b; see also Materials and Methods). Protein yields were excellent (30 mg/L in LB media), with the identity of the construct verified by SDS−PAGE, which also highlights the utility of the dLBT as a co-expression tag for in-gel visualization (Figure 3). Specifically, for confirmation of lanthanide binding, the gel was briefly incubated with Tb^{3+}, and bands containing dLBT were visualized on a UV transilluminator (Figure 3a). The gel was then stained with Coomassie brilliant blue for visualizing total protein (Figure 3b). For corroborating identification, Western blot analysis was carried out, utilizing a monoclonal antibody generated to recognize the sequence IEGDELL (residues 8−14 of **sLBT2**) (Figure 3c). We anticipate that the success of dLBTs as N- and C-terminal tags in these model systems will transfer to other proteins. Despite the increased length (35 residues for **dLBT3**), we have not encountered any additional complications with expression or purification.

Table 2. Sequences of Double-LBTs, along with the Single-LBT That Formed the Basis of the dLBT Design

	residues from protease cleavage[a]	N-terminal binding site	C-terminal binding site
sLBT2			YIDTNNDGWIEGDELLA
dLBT1		YIDTNNDGWIEGDEL	YIDTNNDGWIEGDELLA
dLBT2	G	YIDTNNDGWIEGDEL	YIDTNNDGWIEGDELLA
dLBT3	GPG	YIDTNNDGWIEGDEL	YIDTNNDGWIEGDELLA

[a] The N-terminal glycine on **dLBT2** is residual from the mTEV protease cleavage site, and the corresponding glycine-proline-glycine sequence on **dLBT3** is residual from the DAPase stop site.

Photophysical Characterization. In order to compare the photophysical properties of the newly designed and generated dLBTs with those of the corresponding single-LBTs (sLBTs), luminescence titration (to ascertain maximum intensity and affinity) and terbium-bound water molecule determination was carried out (Table 3). Water molecules directly coordinating the chelated terbium ion cause excited Tb^{3+} to undergo rapid, nonradiative energy transfer to the vibrational states of the water O−H bonds, which is highly detrimental to luminescence.[30] The original screen for brightly luminescent LBTs selected for peptides that, upon chelation, excluded water from the inner coordination sphere. Using methods described in the literature,[23,31,32] it was verified that the water-excluded state was also a property of the dLBTs, shown by near-zero q values in Table 3.

The luminescence intensities of **dLBT2** and **dLBT3**-ubiquitin saturated with Tb^{3+} were compared to those of the correspond-

(30) Horrocks, W. D., Jr.; Sudnick, D. R. *J. Am. Chem. Soc.* **1979**, *101*, 334−340.
(31) Horrocks, W. D., Jr.; Sudnick, D. R. *Acc. Chem. Res.* **1981**, *14*, 384−392.
(32) Beeby, A.; Clarkson, I. M.; Dickins, R. S.; Faulkner, S.; Parker, D.; Royle, L.; de Sousa, A. S.; Williams, J. A. G.; Woods, M. *J. Chem. Soc., Perkin Trans. 2* **1999**, 493−504.

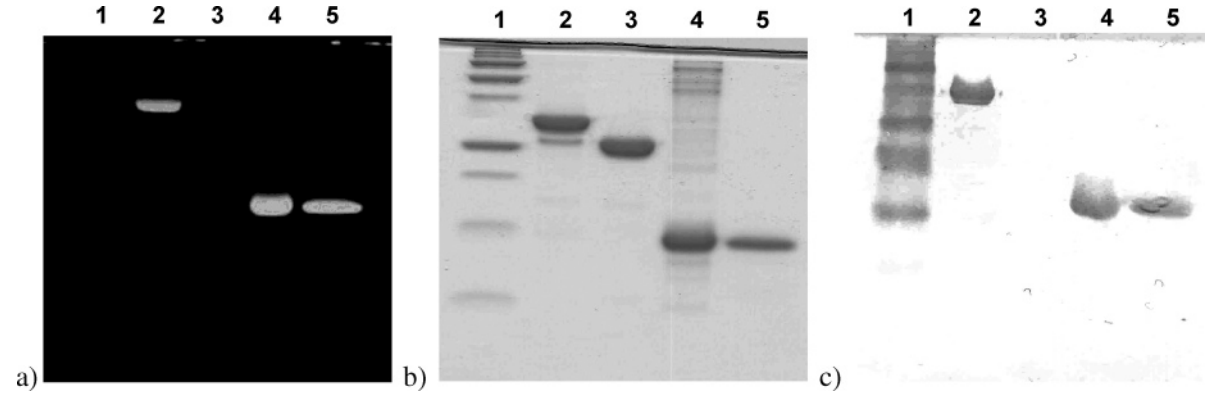

Figure 3. Purification and visualization of the dLBT constructs. For all panels: lane 1, protein mass ladder; lane 2, *GST*-ENLYFQ-**dLBT2**; lane 3, *GST*-ENLYFQ; lane 4, His_6-**dLBT3**-ubiquitin; lane 5, **dLBT3**-ubiquitin. (a) 15% PAGE treated with 4 μM Tb^{3+}, visualized on a UV transilluminator, with enhancement for color and contrast. (b) The same gel, stained with Coomassie brilliant blue. (c) Western blot analysis using a primary LBT-antibody. This figure is shown in color in the Supporting Information, Figure S1.

Table 3. Summary of Photophysical Data

	K_D (nM)					
	direct Tb^{3+} titrations[a]		acetate–buffer Tb^{3+} titrations[a]			
LBT	first metal	second metal	first metal	second metal	relative intensity[b]	q[c]
sLBT2	38		980		1.0	0.08
dLBT2	9.8	35	590	1100	2.1	0.08
dLBT3	3.6	62	570	1000	2.5	0.08
dLBT3-ubiquitin	2.4	23	710	500	3.0	0.05
sLBT1	57[d]		1900		1.9	0.03
GPG-**sLBT1**-ubiquitin	130[d]		4400		1.9	0.13

[a] Dissociation constants were determined by luminescence titration of LBTs by Tb^{3+}, in 100 mM NaCl and 10 mM HEPES buffer (pH 7.0) for direct titrations, or in 100 mM NaOAc and 10 mM HEPES (pH 7.0) buffer for qualitative comparisons (see Materials and Methods). All values are the average of at least three titrations. [b] Luminescence comparison of equal concentrations of peptide or protein construct saturated with Tb^{3+}. [c] The number of bound water molecules, q, was determined by luminescence decay experiments. For a complete summary of experimental details, see the Materials and Methods section. [d] These K_D values are taken from the published data.[22,25]

ing single-LBT at equimolar concentrations (data shown in Table 3). The free peptide **dLBT3**, generated in parallel to **dLBT2**, was also included in this study to assess the effect of the additional N-terminal residues. The peptide **dLBT2** is approximately twice as bright as **sLBT2**, as anticipated. Remarkably, the peptide **dLBT3** is 2.5 times as bright as the prototype **sLBT2**, and the construct **dLBT3**-ubiquitin shows a full 3-fold increase over the original brightness. The reason for this luminescence enhancement is not entirely clear; however, the enhancement is advantageous. It is also noteworthy that neither the N-terminal GPG sequence (as on **dLBT3**) nor the ubiquitin protein results in enhanced LBT luminescence: the construct GPG-**sLBT1**-ubiquitin has a luminescence intensity that is almost identical to that of the **sLBT1** peptide (Table 3).

The terbium affinities were assessed via luminescence titration studies, which reveal that the dLBTs bind with affinity similar to that of the single-LBTs. Two different systems were used for titration experiments at pH 7.0: (1) NaCl/HEPES (used for direct K_D determination[22−24]) and (2) NaOAc/HEPES (used for analysis under competitive conditions). In the latter case, acetate is known to weakly coordinate lanthanides (the 1:1 complex with Tb^{3+} has a K_D of 12 mM);[33] thus, performing titrations in the presence of an acetate buffer artificially weakens the apparent LBT−Tb^{3+} dissociation constant. This enables improved qualitative comparison of the relative K_D values of two tight-binding LBTs or dLBTs. As shown in Table 3, in the direct titrations the binding affinity of dLBTs for the first equivalent of terbium is tighter than that of **sLBT2**; however, the second equivalent binds with comparable affinity to that single-LBT analogue. Whether the first binding event represents binding solely to the N- or C-terminus of the dLBT is unclear. However, in terms of affinity, it has been noted that additional nonligating acidic residues increase affinity, presumably because of bulk electrostatic interactions with the metal ion.[24] Therefore, it is likely that the first terbium-binding event may be promoted by the presence of the negatively charged, unliganded side chains in the remainder of the sequence and that the second binding event is unaffected. In the titrations in acetate buffer, the two dissociation constants are similar, suggesting that the electrostatic effects seen in the direct titrations may be less important. In the acetate buffer (or in the presence of any competing ligand), the LBT binding affinities can be fine-tuned by shifting the equilibrium of high-affinity ligands, which can be an advantage for NMR experiments. It is also noted that the N-terminal residues (G on **dLBT2**, GPG on **dLBT3**) that are necessary consequences of incorporation of the protease cleavage site (Table 2) are not detrimental to binding.

Characterization by NMR. Traditionally, protein structures determined using NMR restraints rely on a large number of short-range distances derived from NOESY experiments and torsion angle restraints determined from vicinal J couplings. More recently, methods have been developed to partially align biomolecules in the magnetic field. This partial alignment leads to residual dipolar couplings (RDCs). The measurement and use of RDCs has become an essential tool for structure determination of proteins.[34−36] Unlike NOEs and scalar ^3J-couplings that report on short-range distances (<5 Å) and

(33) Martell, A. E.; Smith, R. M. *Critical Stability Constants, Vol. 1: Amino Acids*; Plenum Press: New York, 1974; 469 pp.
(34) Tolman, J. R. *Curr. Opin. Struct. Biol.* **2001**, *11*, 532−539.
(35) Lipsitz, R. S.; Tjandra, N. *Annu. Rev. Biophys. Biomol. Struct.* **2004**, *33*, 387−413.
(36) Schwalbe, H.; Grimshaw, S. B.; Spencer, A.; Buck, M.; Boyd, J.; Dobson, C. M.; Redfield, C.; Smith, L. J. *Protein Sci.* **2001**, *10*, 677−688.

dihedral angles, RDCs deliver valuable long-range orientational information. In addition, paramagnetic pseudocontact shifts can be used for the determination of the binding geometry of small ligands to protein receptors.[37]

The introduction of ordered paramagnetic lanthanide ions into proteins allows measurement of RDCs and pseudocontact shifts due to the anisotropic magnetic susceptibility. The residual dipolar coupling of two heteronuclear nuclei P and Q, RDC_{PQ}, depends on the angle θ of the interatomic vector and the external magnetic field B_0:

$$RDC_{PQ} = -\frac{1}{4\pi}\frac{{B_0}^2}{15kT}\frac{\gamma_P\gamma_Q h}{4\pi^2 {r_{PQ}}^3} \times \left[\Delta\chi_{ax}(3\cos^2\theta - 1) + \frac{3}{2}\Delta\chi_{rh}(\sin^2\theta\cos 2\phi)\right]$$

where B_0 is the external magnetic field, k is the Boltzmann constant, T is the temperature in Kelvin, γ_x are the gyromagnetic ratios of nuclei P and Q, h is Planck's constant, r_{PQ} is the distance between P and Q, $\Delta\chi_{ax}$ and $\Delta\chi_{rh}$ are the axial and rhombic components of the magnetic susceptibility tensor, and θ and ϕ are the polar coordinates of the P−Q bond vector in the tensor axis system. In solution, the dipolar coupling is normally averaged to zero due to isotropic molecular tumbling.

Paramagnetic pseudocontact shifts, $\delta\Delta$,[37,38] lead to a change in the observed chemical shifts that depend on distance and position relative to the paramagnetic center:

$$\delta\Delta = \frac{1}{12\pi r^3}\left[\Delta\chi_{ax}(3\cos^2\theta - 1) + \frac{3}{2}\Delta\chi_{rh}\sin^2\theta\cos 2\varphi\right]$$

where $\Delta\chi_{ax}$ and $\Delta\chi_{rh}$ are the axial and rhombic components of the magnetic susceptibility tensor and r, θ, and φ are the spherical coordinates of the nucleus in the frame of the $\Delta\chi$ tensor defined as for the residual dipolar couplings.

Previously, the introduction of an N-terminal sLBT to ubiquitin (as the construct GPG-**sLBT1**-ubiquitin) allowed the analysis of induced RDCs of about 8 Hz at 600 MHz, suggesting some degree of mobility of the LBT relative to the protein.[25] Recently, Otting and co-workers have coupled an sLBT peptide via a disulfide linkage to a cysteine residue in a protein in order to utilize the RDCs and pseudocontact shifts to provide long-range structure information, reporting RDCs of up to 21 Hz at 800 MHz.[26] These studies indicated the utility of the LBTs for the measurement of RDCs; however, there remain opportunities for refining and generalizing the strategy.

NMR analysis was conducted in order to assess the impact of the dLBT on the structure of the conjugated protein. Chemical shift perturbations are powerful tools for determining even very small structural changes.[39] By comparing the ^{1}H and ^{15}N chemical shifts of backbone amide groups of wild-type ubiquitin and the N-terminal **dLBT3**-tagged form of the protein loaded with diamagnetic Lu^{3+}, we can show that the dLBT does not alter the core structure of ubiquitin (Figure 4). Residues in the immediate vicinity of the tag experience small chemical shift changes, while the remainder of the protein stays completely unaffected.

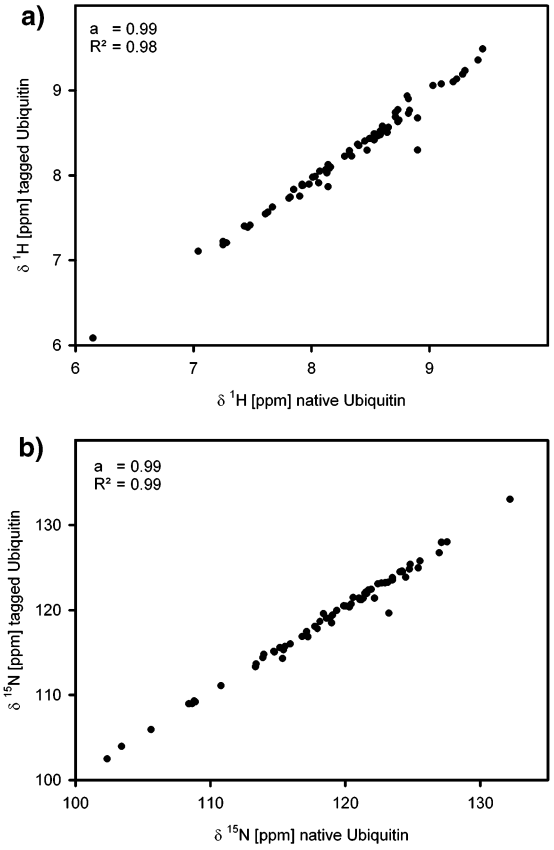

Figure 4. (a) ^{1}H and (b) ^{15}N chemical shifts of **dLBT3**-ubiquitin loaded with Lu^{3+}, plotted against the chemical shifts of native ubiquitin.

The residual dipolar couplings measured at 18.8 T (800 MHz) with thulium (Tm^{3+}) as paramagnetic ion in the **dLBT3**-tagged ubiquitin exceed the values measured in single-LBT-tagged ubiquitin (using GPG-**sLBT1**-ubiquitin, described previously[25]) by a factor of 3, as shown in Figure 5. Approximately 70% of the ubiquitin resonances remained observable. The maximal increase in alignment expected for addition of a second lanthanide-binding site is a factor of 2 for two lanthanide ions with parallel orientation of the axial components $\Delta\chi_{ax}$ of their magnetic susceptibility tensors:

$$\Delta\chi = \Delta\chi^{(A)} + \mathbf{M}_{\alpha,\beta,\gamma}\Delta\chi^{(B)}$$

where $\Delta\chi$ is the resulting paramagnetic susceptibility anisotropy arising from the paramagnetic susceptibility anisotropies of the lanthanide ions $\Delta\chi^{(A)}$ and $\Delta\chi^{(B)}$, each consisting of an axial and a rhombic component,

$$\Delta\chi_{ax} = \chi_{zz} - \frac{\chi_{xx} + \chi_{yy}}{2}$$

$$\Delta\chi_{rh} = \chi_{xx} - \chi_{yy}$$

and **M** is the Euler rotation matrix for rotation around the angles α, β, and γ,

(37) John, M.; Pintacuda, G.; Park, A. Y.; Dixon, N. E.; Otting, G. *J. Am. Chem. Soc.* **2006**, *128*, 12910−12916.
(38) Allegrozzi, M.; Bertini, I.; Janik, M. B. L.; Lee, Y.-M.; Liu, G.; Luchinat, C. *J. Am. Chem. Soc.* **2000**, *122*, 4154−4161..
(39) Shekhtman, A.; Cowburn, D. *Biochem. Biophys. Res. Commun.* **2002**, *296*, 1222−1227.

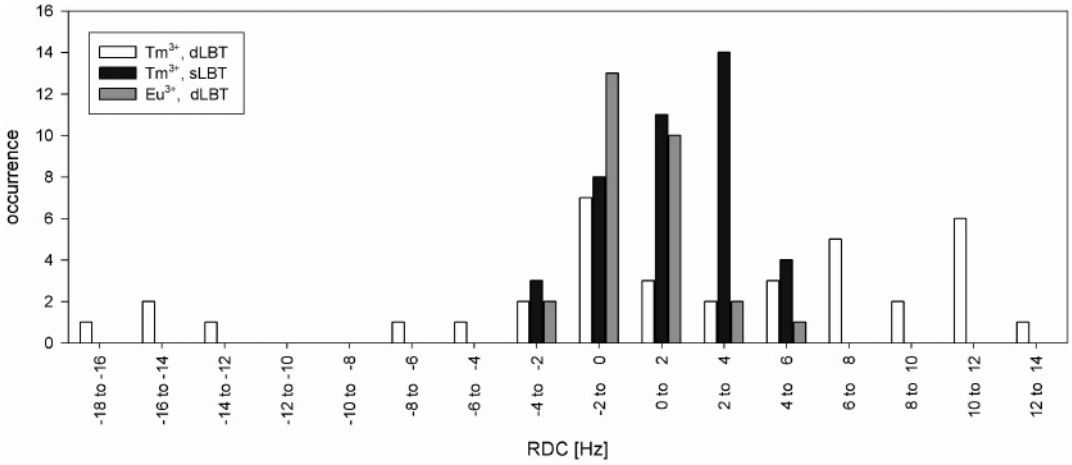

Figure 5. Histogram of RDCs measured with different lanthanide/tag combinations, showing the more than linear increase in RDC size by transition from the sLBT to the dLBT.

$$\mathbf{M}_{\alpha,\beta,\gamma} = \begin{bmatrix} \cos\gamma\cos\beta\cos\alpha - \sin\gamma\sin\alpha & \cos\gamma\cos\beta\sin\alpha + \sin\gamma\cos\alpha & -\cos\gamma\sin\beta \\ -\sin\gamma\cos\beta\cos\alpha - \cos\gamma\sin\alpha & \cos\gamma\cos\alpha - \sin\gamma\cos\beta\sin\alpha & \sin\gamma\sin\beta \\ \sin\beta\cos\alpha & \sin\beta\sin\alpha & \cos\beta \end{bmatrix}$$

Any deviant orientation results in a smaller degree of alignment. Thus, the more than linear increase in the residual dipolar coupling obtained with **dLBT3** must originate from a different source. At the concentrations of protein used in the NMR experiment (~0.5 mM), scaling of the dipolar couplings due to partial binding of the lanthanide can be excluded. Rather, in agreement with the relaxation analysis discussed below, the increase in dipolar couplings likely stems from the reduced mobility of the dLBT relative to the protein. The induced alignment in **dLBT3**-tagged ubiquitin also exceeds that reported from approaches using EDTA-based chelators. Therefore, despite the lower binding affinity of the LBTs relative to those of the synthetic multidentate chelators, the rigid association of the LBT with its attached protein provides a fundamental advantage in the application of the LBTs to the experiments presented. The two LBT modules apparently rigidify one another through a secondary structure that is formed during lanthanide binding. Clearer evidence for this is shown by the crystal structure of **dLBT3**-ubiquitin (in the accompanying paper[29]).

Additional information may be derived by varying the position and the identity of the LBT (single or double). Europium (Eu^{3+}) has a smaller magnetic moment (3.5 μ_B) than the 7.5 μ_B of Tm^{3+}. When Eu^{3+} is used as the paramagnetic ion in **dLBT3**-ubiquitin, RDCs of the same magnitude as those for Tm^{3+} in **sLBT1**-tagged ubiquitin are observed. The alignment tensor generated in the dLBT-tagged protein is found to be linearly independent of the alignment tensor of sLBT-tagged protein (Figure 6a) and therefore yields additional independent structural restraints. Within one type of LBT, different lanthanides induce a similar alignment tensor—shown by the nearly linear distribution in Figure 6b—and therefore produce redundant information. A similar difference in the alignment tensor would also be predicted from the attachment of the LBT to either the N- or the C-terminus of the target protein.

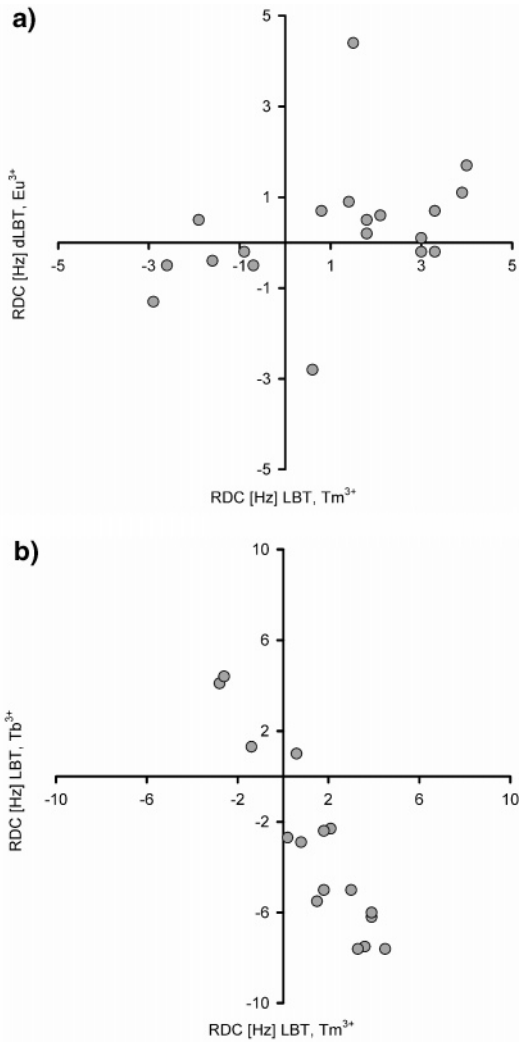

Figure 6. (a) RDCs measured with Eu^{3+} in **dLBT3**, plotted versus RDCs measured with Tm^{3+} in **sLBT1** for different residues, indicating a linearly independent alignment tensor. (b) RDCs measured with Tb^{3+} in **sLBT1**, plotted versus RDCs measured with Tm^{3+} (in the same LBT) for the individual residues, indicating a linearly dependent alignment tensor.

Mean order parameters show that, in terms of minimizing mobility, the dLBT is superior to the sLBT. Spin−lattice and

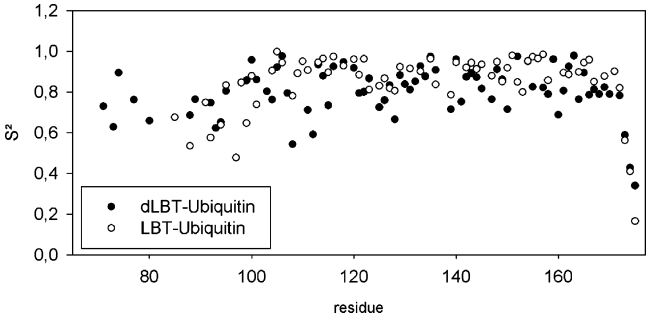

Figure 7. Generalized order parameter S^2 for **dLBT3**-ubiquitin and GPG-**sLBT1**-ubiquitin, showing the higher rigidity of the dLBT. (Residues here are numbered such that the first methionine of ubiquitin is set as M101; the N-terminal residue is G66 for the dLBT construct and G81 for the sLBT construct.)

spin−spin relaxation rates as well as the heteronuclear ^{1}H−^{15}N nuclear Overhauser effect were measured for most backbone amide groups of sLBT- and dLBT-tagged ubiquitin and used to calculate the general order parameter S^2, characterizing the amplitude of intramolecular motion, by a Lipari−Szabo analysis[40,41] with the program TENSOR2,[42] using an anisotropic diffusion tensor (Figure 7).

In the single-LBT, the mean order parameter S^2 for residues of the tag is 0.2 lower than for the core ubiquitin portion of the structure, suggesting a higher flexibility of the tag. In contrast, the mean order parameter S^2 for residues of the tag stays nearly constant for the double-LBT. In **dLBT3**-ubiquitin, the relative mobility of the tag is therefore reduced, consistent with the larger RDC values observed in this system.

Conclusions

We have successfully generated double-lanthanide-binding tags of fewer than 40 amino acids, capable of simultaneously binding two lanthanide ions. The peptides **dLBT2** and **dLBT3** have been expressed as C-terminal fusions to GST and then cleaved to yield free peptides, which were photophysically characterized to reveal that the concatenation of two LBTs resulted in superior binding and luminescence properties. When **dLBT3** was expressed as an N-terminal ubiquitin construct, the lanthanide-binding and luminescence characteristics of dLBTs were improved. NMR studies on the **dLBT3**-tagged ubiquitin reveal that, in addition to the improved photophysical properties, the efficiency of the tag in mediating alignment between the lanthanide ions and the protein is increased dramatically by the lower mobility of the dLBT. This finding now inspires implementation of the dLBT to solve the phase problem for crystallographic structure determination (as in the accompanying paper[29]), which together with the extension of applications for luminescence and NMR is the focus on continuing efforts. The dLBT adds a unique, versatile tool that enables new approaches for the study of the structure, function, dynamics, and interactions of proteins.

Materials and Methods

Luminescence Titrations. Titrations were recorded on a Jobin Yvon Horiba Fluoromax-3 spectrometer in a 1 cm path length quartz cuvette. Tryptophan-sensitized Tb^{3+} luminescence was collected by exciting the sample at 280 nm and recording emission at 544 nm; a 315 nm long-pass filter was used to avoid interference from harmonic doubling. Slit widths of 5 nm were used, with 1 s integration times. Spectra were recorded at room temperature and were corrected for intensity using the manufacturer-supplied correction factors. Peptide or protein solutions were prepared in 3 mL of buffer (pH 7.0). For direct titrations, the buffer was 100 mM NaCl and 10 mM HEPES (*N*-2-hydroxyethylpiperazine-*N*′-2-ethanesulfonic acid, pH 7.0). For "relative" (qualitative comparison) titrations, the buffer was 100 mM NaOAc and 10 mM HEPES (pH 7.0). The peptide or protein concentration of the stock solutions used in photophysical experiments was determined by UV absorption at 280 nm in a 6 M guanidinium chloride solution using known extinction coefficients of Trp and Tyr residues.

Tb^{3+} stock solutions were prepared from the $TbCl_3$ hydrate salts (Sigma-Aldrich) as ∼50 mM solutions in 1 mM HCl and were diluted as needed. Exact concentrations were determined by colorimetric titrations using a standardized EDTA solution (Aldrich) and a Xylenol Orange indicator as described in the literature.[43] Aliquots of Tb^{3+} were added to a solution of peptide or protein (50 nM for direct titrations, 100 nM for titrations in acetate). For direct titrations, after a background data point was obtained, seven 1 μL aliquots of 40 μM Tb^{3+} were added, followed by three aliquots of 1 μL of 100 μM Tb^{3+} and three aliquots of 1 μL of 200 μM Tb^{3+}. After each addition, the solution was mixed and a data point taken. Relative titrations were conducted in the same manner, except with six aliquots of 1 μL of 100 μM Tb^{3+}, seven aliquots of 1 μL of 200 μM Tb^{3+}, and five aliquots of 1 μL of 1 mM Tb^{3+}. Comparative luminescence intensities of single- and double-LBTs saturated with Tb^{3+} were determined under the same conditions, at concentrations of 200 nM peptide or protein and 500 nM Tb^{3+} (for single-LBTs) or 1 μM Tb^{3+} (for double-LBTs).

Luminescence titration spectra obtained in this fashion were analyzed with the program SPECFIT/32,[44] which determines log β values (where β is the binding constant) using the equilibrium data. Calculated log β values were then translated into the dissociation constants ($K_D = 10^{-\log \beta}$). For two-site calculations, luminescence of the 1:1 complex was assigned to be half the luminescence of the 2:1 complex.

Determination of Tb^{3+}-Bound Water Molecules. Luminescence lifetimes were measured in a Jobin Yvon Horiba Fluoromax-3 spectrometer, equipped with a Spex 1934D3 phosphorimeter. Samples were excited by a pulse of 280 nm light for 70 ms. Data were collected at 544 nm for 15 ms in 30 μs increments following a 50 μs delay. Slit widths were 5 nm for excitation and 10 nm for emission. Samples were 2 μM peptide or protein, with 2.5 equiv of Tb^{3+}, in 100 mM NaCl and 10 mM HEPES (pH 7.0) in a 500 μL cuvette. Data sets were fit to a single-exponential decay, and lifetimes in varying percentages of D_2O (Cambridge Isotope Laboratories) were plotted on a curve to determine the lifetimes in pure H_2O and pure D_2O. The number of Tb^{3+}-bound water molecules, q, could then be calculated using the equation $q = A'_{Tb}(1/\tau_{H_2O} - 1/\tau_{D_2O} - 0.06)$ as described in the literature, where $A'_{Tb} = 5$ ms, τ is the lifetime in the specified solvent, and -0.06 ms^{-1} is the correction factor for outer-sphere water molecules.[32]

NMR Experiments. NMR experiments were conducted in buffer (20 mM HEPES, pH 7, with 100 mM NaCl). Samples were prepared by dilution of protein solution to below 100 μM protein, followed by slow addition of 2.3 equiv of lanthanide ($LnCl_3$) solution. After a buffer exchange to remove excess lanthanide ion, the protein was concentrated to about 500 μM using Amicon Centriprep/Centricon centrifugal concentrator devices. ^{15}N HSQC spectra were recorded using 2048 × 256 data points in t_2 and t_1, respectively, spectral widths of 14 × 32

(40) Lipari, G.; Szabo, A. *J. Am. Chem. Soc.* **1982**, *104*, 4546−4559.
(41) Lipari, G.; Szabo, A. *J. Am. Chem. Soc.* **1982**, *104*, 4559−4570.
(42) Dosset, P.; Hus, J.-C.; Blackledge, M.; Marion, D. *J. Biomol. NMR* **2000**, *16*, 23−28.
(43) Pribil, R. *Talanta* **1967**, *14*, 619−627. .
(44) Binstead, R.; Jung, B.; Zuberbühler, A. *SPECFIT/32 for Windows*, Version 3.0.38; Spectrum Software Associates: Marlborough, MA, 2000. SPECFIT provides global analysis of equilibrium and kinetic systems using singular value decomposition and nonlinear regression modeling by the Levenberg−Marquardt method.

ppm in ω_2 and ω_1, and eight scans per t_1 increment on a Bruker AV800 spectrometer equipped with a 5 mm TXI CryoProbe $^1H\{^{13}C/^{15}N\}$ with Z-gradient at 298 K. Nonspecific lanthanide binding was not observed.

RDCs were obtained by subtraction of the scalar $^1J(H^N,N)$ coupling of the superposition of scalar and dipolar coupling, both measured in not-proton-decoupled ^{15}N HSQC spectra. They were recorded with 1024 $\times$ 768 complex data points in t_2 and t_1, respectively, spectral widths of 14 $\times$ 32 ppm in ω_2 and ω_1, and 32 scans per t_1 increment on a Bruker AV800 spectrometer equipped with a 5 mm TXI CryoProbe $^1H\{^{13}C/^{15}N\}$ with Z-gradient at 298 K. Scalar couplings were measured using diamagnetic lutetium (Lu^{3+}), whereas paramagnetic thulium (Tm^{3+}) was used for RDC measurements.

^{15}N spin−lattice relaxation rates were obtained using relaxation delays of 20, 50, 75, 100, 200, 400, 500, 600, 700, 800, 900, 1000, 1200, and 1500 ms. For measurement of ^{15}N spin−spin relaxation rates, delays of 18, 36, 54, 72, 90, 108, 126, 144, 162, 180, 198, 216, 234, 252, 270, 288, 324, 342, 360, 378, 396, and 414 ms were used. The spectra were recorded at 298 K using 2048 $\times$ 256 data points in t_2 and t_1, respectively, spectral widths of 14 $\times$ 32 ppm in ω_2 and ω_1, and eight scans per t_1 increment on Bruker DRX600 spectrometers equipped with a 5 mm TXI CryoProbe $^1H\{^{13}C/^{15}N\}$ with Z-gradient for **dLBT3**-ubiquitin and a 5 mm TXI RT $^1H\{^{13}C/^{15}N\}$ with Z-gradient for GPG-**sLBT1**-ubiquitin.

The $^1H-^{15}N$ NOE was measured interleaved, using 2048 $\times$ (2 $\times$ 384) data points, spectral widths of 14 $\times$ 32 ppm, and eight scans per t_1 increment on Bruker DRX600 spectrometers with a 5 mm TXI CryoProbe $^1H\{^{13}C/^{15}N\}$ with Z-gradient for **dLBT3**-ubiquitin and a 5 mm TXI RT $^1H\{^{13}C/^{15}N\}$ with Z-gradient for single-LBT-ubiquitin.

Acknowledgment. This research was supported by a NSF-CRC program grant to B.I., K.N.A., and H.S. (CHE-0304832). Work has also been supported by the state of Hesse (Center for Biomolecular Magnetic Resonance) and by the EU SPINE project.

Supporting Information Available: Protocols for peptide synthesis, cloning, protein expression and purification, protease cleavage, PAGE analysis, and NMR relaxation data. This material is available free of charge via the Internet at http://pubs.acs.org.

JA070480V